Applied Geochemistry 147 (2022) 105482

Contents lists available at ScienceDirect

Applied Geochemistry

journal homepage: www.elsevier.com/locate/apgeochem

Soil core study indicates limited CO_2 removal by enhanced weathering in dry croplands in the UK

F.L. Buckingham [a,*], G.M. Henderson [a], P. Holdship [a], P. Renforth [b]

[a] Department of Earth Sciences, University of Oxford, Oxford, OX1 3AN, UK
[b] School of Engineering and Physical Sciences, Heriot-Watt University, Edinburgh, EH14 4AS, UK

ARTICLE INFO

Editorial handling by Prof. M. Kersten

Keywords:
Enhanced weathering
Terrestrial weathering
Negative emissions
Carbon dioxide removal

ABSTRACT

The application of crushed silicate minerals to agricultural soils has been suggested as a route to enhance weathering rates and increase CO_2 drawdown. Laboratory studies have attempted to evaluate the potential of enhanced weathering as a CO_2 removal technique but do not simulate the geochemical complexity of soil environments, and studies in the field are limited in the nature of data they can collect. To overcome these limitations, this study uses an experimental set-up which fully encapsulates field conditions in a controlled setting using soil cores removed from UK cropland and treated with crushed basalt. Cores were exposed to natural weather conditions throughout a 14-month time series, and soil solution was sampled in 10–20 cm intervals in the core to provide insight into the fate of dissolution products with soil depth.

This study assessed the rate and chemistry of basalt dissolution 8 months after addition at a high application rate (100 t basalt ha^{-1}) using direct measurements from a UK soil. Assuming conclusions drawn from this study are representative of field-scale enhanced weathering, findings indicate that a set application of basalt to lime-rich, unirrigated UK soils releases alkalinity at a rate of 310 ± 30 eq ha^{-1} yr^{-1} and could remove 10.2 ± 0.8 $kgCO_2$ ha^{-1} yr^{-1}. Accumulation of undissolved basalt may also lead to large and irreversible changes to soil compositions following repeated application. When considering variation in hydrology around the UK, we assess the drawdown potential of application of basalt to all UK arable land as 1.3 ± 0.1 $MtCO_2$ yr^{-1} which is equivalent to 3% of current UK agricultural CO_2 emissions. This is 5- to 25- fold slower than previous modelled assessments, likely due to complexities of soil systems and to water limitation on alkalinity release. Further research is needed to fully assess controls on the potential of enhanced weathering in the real-world environment, across a range of hydrological and soil environments, before the approach is substantively scaled-up for CO_2 removal.

1. Introduction

Carbon dioxide removal technologies, such as enhanced weathering, are heavily relied upon to meet the international target of limiting global average temperature rise to 2 °C. These targets will require several hundred $GtCO_2$ to be removed from the atmosphere by the end of the century (e.g., Fuss et al., 2018; The Royal Society and Royal Academy of Engineering, 2018). Terrestrial enhanced weathering (EW) involves the application of crushed rocks or minerals to agricultural land to accelerate natural weathering and CO_2 drawdown via the release of alkalinity (Seifritz, 1990; Hartmann et al., 2013 and references therein). During terrestrial chemical weathering, dissolution of minerals by carbonic acid in soil solution leads to the release of cations. This increases total alkalinity and draws down CO_2 into dissolved inorganic carbon (Eq. (1)) (Walker et al., 1981; Berner, 1999). The majority of DIC exists as bicarbonate ions (HCO_3^-) in water of pH 6–9; whereby the input of 1 mol of divalent cation is balanced by the production of approximately 2 mol of bicarbonate ions and removal of approximately 2 mol of carbon from the atmosphere. Precipitation of carbonates in soils and freshwater environments sequesters carbon, but this process drives the outgassing of CO_2 and reduces the sequestration potential from silicate dissolution by half (Eq. (2)) (Manning, 2008). The net effect of weathering on carbon drawdown is therefore greatest if sequestered carbon remains in a dissolved form.

$$Mg_2SiO_4 + 4CO_2 + 4H_2O \rightarrow 2Mg^{2+} + 4HCO_3^- + H_4SiO_4 \quad (1)$$

* Corresponding author.
E-mail address: frances.buckingham@earth.ox.ac.uk (F.L. Buckingham).

https://doi.org/10.1016/j.apgeochem.2022.105482
Received 3 July 2022; Received in revised form 8 October 2022; Accepted 10 October 2022
Available online 17 October 2022

$$2Mg^{2+} + 4HCO_3^- + H_4SiO_4 \rightarrow 2MgCO_3 + 2CO_2 + 4H_2O + SiO_2 \quad (2)$$

Previous calculations suggest enhanced weathering could remove 0.5–4 $GtCO_2\ yr^{-1}$ globally by the end of this century (Smith et al., 2015). However, existing pot (ten Berge, 2012; Amann et al., 2020; Kelland et al., 2020), core (Renforth et al., 2015), laboratory (Palandri and Kharaka, 2004) and modelling studies (Strefler et al., 2018; Beerling et al., 2020; Kantzas et al., 2022) produce conflicting estimates for rock and mineral dissolution rates and the carbon dioxide removal (CDR) potential of enhanced weathering – see Swoboda et al. (2021) for a full discussion. Field studies are inherently costly and time consuming, and it is difficult to isolate variables which impact the dissolution process. In comparison, laboratory dissolution experiments oversimplify the complexities of the natural soil environment and fail to represent factors which influence mineral-fluid interaction, such as: preferential flow, surface passivation, and saturation in micropores (White and Brantley, 2003). Consequently, the rate of olivine dissolution calculated from laboratory studies (10^{-14} mol(Olivine) $cm^{-2}\ s^{-1}$, 19°) (Palandri and Kharaka, 2004) is up to three orders of magnitude faster than olivine dissolution measured in treated pot and core studies ($10^{-17.12}$ to $10^{-17.75}$ mol(Olivine) $cm^{-2}\ s^{-1}$, Amann et al., 2020; $10^{-16.7}$ to $10^{-15.8}$ mol(Olivine) $cm^{-2}\ s^{-1}$, Renforth et al., 2015). Furthermore, existing pot and core studies control temperature and irrigation rate and therefore fail to capture the extent to which natural drying/wetting cycles influence mineral saturation and dissolution rate. The lack of depth-resolution in previous pot and core studies make it difficult to understand the intricacies of dissolution in a soil environment where the distribution of dissolution products are influenced by downwards percolation, secondary mineralisation, adsorption and exchange.

Unlike the fast-weathering mineral olivine, which is known to release Ni and Cr into the soil (Renforth et al., 2015), basalt rock has been proposed as an ideal treatment for enhanced weathering as its application to agricultural soils is an established practice which provides essential nutrients (Beerling et al., 2020). Although basalt has low levels of heavy metals, it is composed of a range of minerals with varying dissolution rates. It is therefore important to assess whether trace quantities of fast-weathering, metal-rich minerals within basalt release heavy metals into the soil-water environment. The dissolution rate of basalt ($10^{-15.3}$ to $10^{-16.2}$ mol(Ca) $cm^{-2}\ s^{-1}$) has previously been measured in a comprehensive pot study by Kelland et al. (2020); however, to date, the CDR potential of basalt has not been adequately assessed in an environment representative of natural hydrological and soil conditions.

In this study, we use soil cores removed from UK cropland and develop a robust method of extracting sufficient soil solution for geochemical analysis. Coarse-grained basalt was applied at a rate equivalent to 100 t ha^{-1} in-line with a recent mesocosm study (Kelland et al., 2020). Soil solution was sampled at up to 10 depths through a 1.0 m length core, providing a high resolution insight into ion release and the fate of dissolved products in the soil. We simulate the field environment by exposing cores to real-time variations in weather and temperature, and overcome low pore-water saturation with a well-characterised irrigation regime. Chemical measurements of soil solution sampled 8 months after basalt application provide the rate of basalt dissolution, alkalinity release and the CO_2 sequestration potential of basalt in agricultural soils.

2. Methods

2.1. Experimental design

Soil cores were used in this study to addresses the limitations of laboratory experiments, which simplify the complexity of the soil environment, and field studies, which are inherently costly, time-consuming, difficult to replicate, control and monitor. In August 2018, 36 soil cores of 1.0 m length and 0.1 m diameter containing lime-rich loamy soil were extracted from an agricultural field in North Oxfordshire (FAI Farm, Wytham, 51.781°, −1.3141°) that had most recently been used to cultivate *Avena sativa* (oats) and *Hordeum vulgare* (barley). Soil cores were held in transparent plastic core liners during transport and, in most cases, throughout the experimental work. The bulk mineralogy, elemental composition and physical properties of one soil core was measured at the beginning of the study. From August 2018 the remaining cores were stored vertically on the roof of the Earth Sciences Department at the University of Oxford and wrapped in black sheeting. The tops of all soil cores were exposed to local weather and temperature to permit continued soil weathering in an outside environment prior to soil solution sampling. Herbaceous flowering plants naturally grew in the soil cores and were neither removed nor measured.

Soil cores were left undisturbed for three months before six cores were used during this study from Nov'2018 to Jan'2020. Rhizon CCS samplers with a 0.15 μm pore size (Rhizosphere Research Products) were inserted horizontally every 10 cm–20 cm along the profile of the core. Effluent collected into amber LDPE bottles at the base of the core (Figs. 1–2) and is hereafter reported as soil solution collected at 100 cm. In this way, soil solution could be sampled throughout the time series from a range of depths without disrupting the structure of the soil core. Basalt was mixed into three soil cores in Feb'2019. The top 13 cm of three cores was removed, mixed thoroughly with crushed basalt (125–250 μm) at a rate equivalent to 100 t ha^{-1}, and returned to the respective core. Three control cores were treated to identical mixing but without basalt addition. This high application rate is aligned with a basalt-treated mesocosm study by Kelland et al. (2020) (100 t ha^{-1}), is lower than used in an olivine-treated core study (127 t ha^{-1}; Renforth et al., 2015), and is larger than applied in a modelling study (40 t ha^{-1}) (Kantzas et al., 2022). Changes in the dissolved soil water chemistry directly associated with basalt dissolution were isolated by comparing the concentration measured in the treated cores and control cores.

Water sampling commenced in October 2019, 8 months after basalt addition, and continued until January 2020. This interval allowed for equilibration of the basalt in the mixed layer. Sampling occurred approximately fortnightly with a five week interval between Dec'2019 and Jan'2020. Immediately before sampling, cores were irrigated with 330 ml rainwater (collected immediately adjacent to the cores) with added uranine powder to create a fluorescent dye (50 μg ml^{-1}). This increased pore saturation and permitted recovery of fluid. Rhizon samplers were held under vacuum for 5 hrs during sample collection. The concentration of dissolved ions in soil solutions samples were corrected for dilution experienced during irrigation using fluorescent uranine dye concentrations in extracted fluids (see SI for a full description). Natural rainfall was the only additional flux through the core over the remainder of the study; therefore the infiltration flux was calculated from rainfall minus evapotranspiration (Eq.S2, SI) (1.2 ml day^{-1}; 57 mm yr^{-1}; 1.4×10^{-5} g s^{-1}). The cation concentration of rainfall was less than 5% of soil solution and was accounted for in the dilution correction (see SI). It is possible rainwater added during sampling introduced acidity to the soil-water system. However, this is unlikely to have substantially enhanced mineral dissolution within the 5 hr window the additional rainwater took to percolate through the core (see S3 for further details).

This experimental set-up aims to represent field conditions as much as possible; however conclusions are sensitive to the design of the core study. For example, CO_2 partial pressure and fluid drainage may differ between the core and field environment. In addition, TIC and pedogenic carbonate formation were not assessed within the scope of this study and could influence the net CDR potential of EW. This study examines carbon drawdown in soils extracted from a single field site exposed to local weather conditions; therefore appropriate caution should be applied when extrapolating findings to the field scale which include a range of soil types, hydrological and climate conditions. Further EW trials will be required to overcome these knowledge gaps and permit a robust understanding of the efficacy of EW across a range of environments. The experimental set-up developed in this study formed the foundation of a

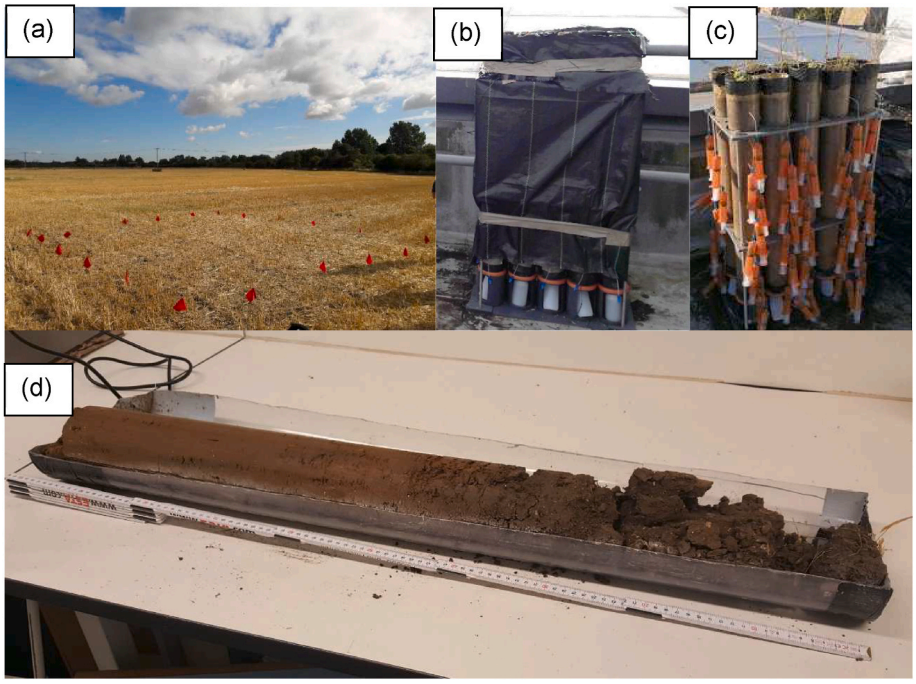

Fig. 1. Experimental set-up. (a) 6 × 6 m wide sampling site where 36, 1.0 × 0.1 m diameter soil cores were extracted; FAI Farms, Oxfordshire, UK (Aug'18). (b) Soil cores installed on the roof of the Earth Sciences Department after extraction, covered in black sheeting. Six cores were used in this study and additional cores were used as part of a wider study. (c) Syringes attached to Rhizon samplers under vacuum during sampling. (d) An untreated soil core (Nov'18).

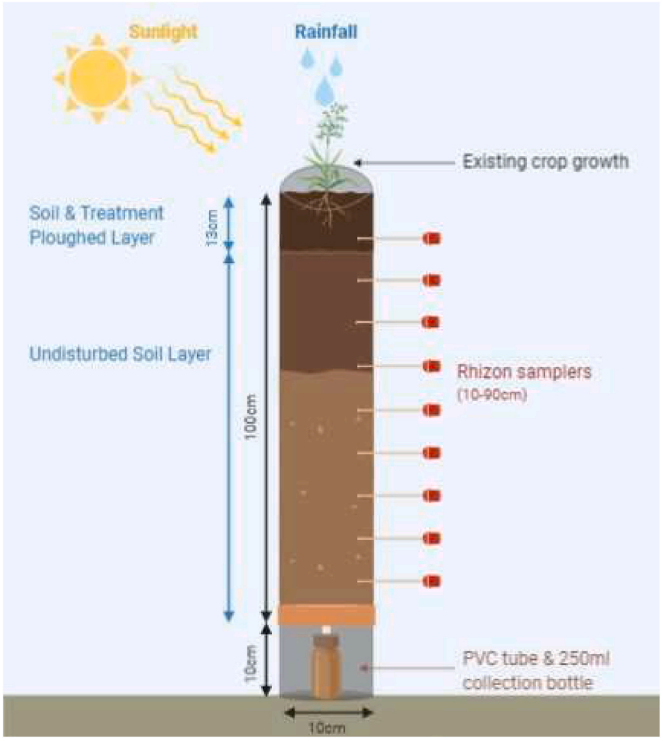

Fig. 2. Schematic depiction of the experimental set up.

wider soil core study to assess a range of possible materials for enhanced weathering in addition to basalt.

2.2. Soil and basalt characterisation

An untreated soil core was cut into 10 cm sections at the beginning of the study (Nov'18), oven dried at 60 °C for 48 h, crushed using a jaw crusher and powdered on a Tema mill (University of Oxford). Soil samples were analysed for bulk density, moisture content, total inorganic carbon content (TIC), total organic carbon content (TOC), bulk mineralogy (XRD) and elemental composition (XRF) (University of Cardiff, University of Oxford) - see SI for further details. The characteristics of the soil distinctly changed over the 1m soil profile (Table S1); for example, TOC was highest above 30 cm (2.5%), compared to an average of 1.5% across the remainder of the core. TIC and calcite measured with XRD exhibited a broadly consistent relationship with depth, whereby the average TIC above 20 cm was 4-fold lower than below 80 cm. Soil mineralogy is detailed in Table S2 and comprises noteable (>10%) calcite, Fe-oxide, Al-oxide and SiO_2. Calcite, measured with XRD, reduced from 3% above 40 cm to 0% between 40 and 60 cm, and increased to 10% below 80 cm.

Basalt was obtained from the Cascade Mountain Range, Oregon (Central Oregon Basalt Products) and crushed to a fine powder on a Tema mill (University of Oxford). The 125–250 μm size fraction was extracted with a series of dry sieves. The BET surface-area (16.3 ± 0.2 $m^2\ g^{-1}$) of the 125–250 μm size fraction was determined by N_2 adsorption using Micromeretics Gemini VI (Oxford). The geometric surface-area was calculated in accordance with Tester et al. (1993) (0.011 $m^2\ g^{-1}$) (Eq.S4, SI). XRF analysis was conducted using a Rigaku ZSX Primus II with a pre-calibrated EZ-scan semi quant program, calibrated using BCR-1 and 879-1 standards (Leeds University) (Table 1). The mineralogy of basalt sourced from the same region as the basalt applied in this study is comprehensively described in Kelland et al. (2020).

2.3. Sampling protocol

Throughout the study, the top surface of all six soil cores was exposed to natural rainfall. Rainfall was measured at the site (Department of Earth Sciences, University of Oxford; Feb'19-Jan'20) and is similar to that observed nearby at Chimney Meadows, Oxfordshire (1.8 mm day^{-1}, 14 ml day^{-1} $core^{-1}$) (UKCEH, 2021). After evapotranspiration, the cores

Table 1
Composition of applied basalt, and soil. Soil samples were measured at the beginning of the study and averaged over the 1 m soil core.

	Crushed Basalt	Initial soil
BET surface area ($m^2\ g^{-1}$)	16.3 ± 0.2	
Geometric surface area ($m^2\ g^{-1}$)	0.011	
Particle size (μm)	125–250	
XRF analysis	Mass %	
Al_2O_3	13.1 ± 0.5	13.2 ± 0.5
BaO	0.10 ± 0.04	
CaO	9 ± 1	15 ± 2
Fe_2O_3	18.9 ± 0.5	12.0 ± 0.3
K_2O	2 ± 1	3 ± 2
MgO	1.5 ± 0.9	0.9 ± 0.5
MnO	0.29 ± 0.02	0.20 ± 0.01
Na_2O	1.8 ± 0.8	0.14 ± 0.06
P_2O_5	0.46 ± 0.02	0.65 ± 0.03
SiO_2	49 ± 5	53 ± 5
TiO_2	3.0 ± 0.8	1.1 ± 0.3
V_2O_5	0.11 ± 0.02	0.034 ± 0.005

normally contained insufficient water to recover soil solution samples from the Rhizons or from effluent at the base. To permit sampling, each soil core was therefore also irrigated on each of the five sampling occasions (Oct'2019–Jan'2020) with an additional 330 ml of rainfall (collected adjacent to the core) with added fluorescent dye (see S1 for full details of this process). This sampling protocol proved the most efficient means of maintaining natural hydrological conditions throughout the majority of the time-series whilst increasing the number and volume of soil solution samples. Immediately after irrigation, 50 ml BD Plastipak amber luer lock syringes were attached to Rhizon samplers under vacuum. Cores were left for 5 h before soil solution was collected. Based on time-series measurement of the fluorescent dye this is sufficient time for the added rainwater to increase pore saturation through the core (see S3 for further details).

The fluorescence and concentration of uranine in each soil solution sample was measured with a SPARK fluorimeter. The ratio of the concentration of uranine in the soil solution sample relative to the fluorescent dye was used to calculate the extent pore-water was diluted with fluorescent dye on a sample-by-sample basis. See S2 for further details.

2.4. Soil solution analysis

The concentrations of major and trace elements in the soil solution samples were determined using a PerkinElmer NexION 350D inductively coupled plasma mass-spectrometer (ICP-MS) (University of Oxford), which was calibrated using externally prepared calibration standards (Merck Certipur ICP Standards), and corrected for any drift by internal standard additions of Rh, In, Re and Ir into all measured solutions. Accuracy was assessed by analysing the international reference standard for pore-waters (SLRS-6) and varied from ±6–11%. Soil solutions were diluted 50-fold in a metal-free laboratory with 2% HNO_3 before the analysis of major elements (Ca, Mg, K, Na). The remaining soil solution was diluted to 3 ml and analysed for trace metals.

3. Results

3.1. Ion release

To prevent sampling depth biasing the concentration of dissolved ions averaged over the whole soil core, the concentration of dissolved ions were first averaged in depth sections corresponding to distinct soil zones (top, 0–30 cm; middle 40–60 cm; base, 70–100 cm). The concentration of each ion was averaged for the three depth ranges for the five sampling events and for the triplicate cores (treated and control). The dissolved concentration of Ca, Cr, K, Na, Mg and Sr averaged across the whole length of triplicate cores was significantly elevated in basalt-treated cores (Fig. S3). This differs from results by Kelland et al. (2020) who observed no significant increase in dissolved Ca and Si.

Differences in the average values of dissolved ions between the treated and control cores are normalised to the percent concentration in basalt to assess the impact of basalt dissolution (Fig. 3). The dissolved concentrations of Ca, K, Na and Mg were elevated in basalt-treated soil solutions and were notably higher at the top of cores localised to the area of basalt addition. In contrast, soil solutions averaged over the whole length of basalt-treated cores were depleted in Fe, Al, (−1 pbb/wt%), Mn (−2 ppb/wt%) and Si (- 20 pbb/wt%). Ca was notably depleted at the base of the core, indicative of secondary carbonate formation following solution saturation.

4. Discussion

4.1. Ion release rate

A key goal of this study is to assess the rate of release of elements from the added basalt into the pore-waters in the core; both those elements that will consume CO_2, and those that may have negative consequences (e.g. through their toxicity). The surface-area-normalised ion release rate, $Wr_{surface\ area}$, of each element (mol(ion) $cm^{-2}\ s^{-1}$) was calculated using eq. (3);

$$Wr_{surface\ area} = \frac{([C]_{treated-control}) \cdot Q}{SA_{basalt} \cdot M_{basalt}} \quad (3)$$

where Q is the infiltration flux through the core, calculated from rainfall minus evaporation (1.4×10^{-5} g s^{-1}); C is the dissolved molar concentration in soil pore-waters of each ion averaged across the whole length of triplicate cores for the five sampling events (mol g^{-1}); SA_{basalt} is the BET surface-area of basalt (16.3×10^4 $cm^2\ g^{-1}$); and M_{basalt} is the mass of basalt applied (79 g). Ions released from basalt dissolution were isolated by subtracting the concentration of ions in control cores from the concentration in treated cores.

BET surface area was used for surface-area normalisation so our results can be readily compared to previous studies (Renforth et al., 2015; Amann et al., 2020; Kelland et al., 2020). We recognise the limitations of normalising to the BET surface area of crushed rock which are discussed in depth by other authors (Brantley and Mellot, 2000; Kelemen et al., 2020). This uncertainty in surface-area normalisation does not influence the rate of alkalinity release per hectare for a given mass of basalt addition, and therefore does not influence the calculation of CO_2 sequestration below.

The release of ions from basalt in soil varies from 19×10^{-20} mol(Ca) $cm^2\ s^{-1}$ to -$8x10^{-24}$ mol(Mn) $cm^2\ s^{-1}$ (Table 2). The negative release rate of some ions implies removal of these elements from solution, presumably into secondary phases. For example, the concentration of dissolved Si is lower in basalt-treated cores, relative to the control, and is consistent with an olivine-treated pot study by Amann et al. (2020). These findings suggests EW will not contribute to an elevated land-ocean Si flux as suggested by other authors (Hartmann et al., 2013).

The surface-area-normalised release rate of Ca and Mg in Kelland et al. (2020) was ~3 orders of magnitude faster than release into the dissolved phase in this soil core study (Fig. 4). Kelland et al. (2020) sourced basalt from the same region as in this study (Cascade Mountain Range, Oregon) and also applied basalt at 100 t ha^{-1}, so the discrepancy in ion release rate is thought to relate to other differences in the experimental set-up. For example, Kelland et al. (2020) assessed dissolution by measurement of the soil-water-plant phase, therefore uptake into the exchangeable pool and plant phase may partially explain the difference. The Kelland et al. (2020) experiment also used a higher water flux (767 mm yr^{-1}) than the natural flux of this study (57 mm yr^{-1}) which will further contribute to high dissolution rates (as discussed in Section 4.5 below).

Basalt applied in this study contained ~30-fold less Mg (0.9 wt% Mg)

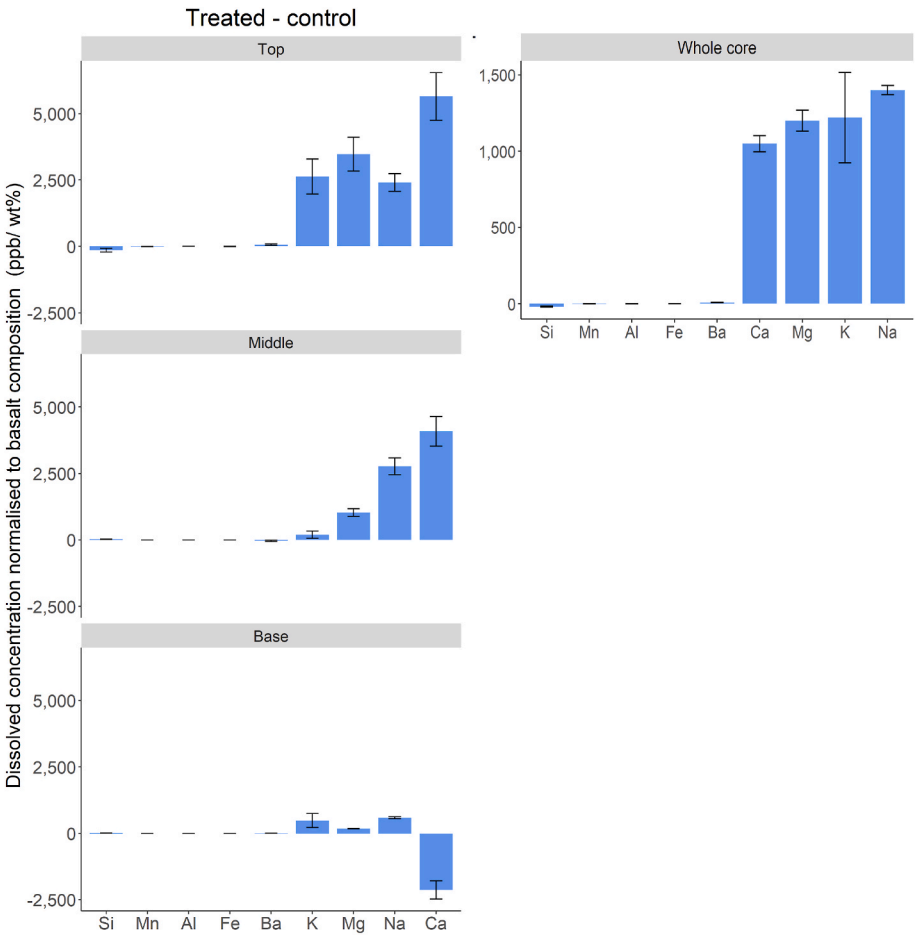

Fig. 3. The difference in ion concentrations in basalt-treated and control cores. Shown is the average concentrations over five-sampling events in the top (0–30 cm), middle (40–60 cm), base (70–100 cm) and whole core (0–100 cm) for the three treated cores, minus the average for the three control cores (μg L^{-1}), normalised to the percent concentration of the respective element in basalt. Values above zero are attributed to basalt dissolution, with the magnitude indicating the relative release to the dissolved phase of each element. Uncertainty shown is based on the standard error over three treated and three untreated cores.

Table 2
BET surface-area-normalised ion release rate (mol cm^{-2} s^{-1}) of elements in basalt-treated cores. Negative rates indicate removal of the respective element from solution.

	Ion release rate (mol cm^{-2} s^{-1})
Al	$-24 \times 10^{-23} \pm 4 \times 10^{-23}$
Ba	$6 \times 10^{-24} \pm 1 \times 10^{-24}$
Ca	$19 \times 10^{-20} \pm 1 \times 10^{-20}$
Cr	$30 \times 10^{-25} \pm 3 \times 10^{-25}$
Fe	$-19 \times 10^{-24} \pm 6 \times 10^{-24}$
K	$6 \times 10^{-20} \pm 1 \times 10^{-20}$
Mg	$49 \times 10^{-21} \pm 3 \times 10^{-21}$
Mn	$-8 \times 10^{-24} \pm 3 \times 10^{-24}$
Na	$72 \times 10^{-21} \pm 2 \times 10^{-21}$
Ni	$26 \times 10^{-25} \pm 2 \times 10^{-25}$
P	$-9 \times 10^{-21} \pm 3 \times 10^{-21}$
Si	$-18 \times 10^{-21} \pm 4 \times 10^{-21}$
Sr	$42 \times 10^{-23} \pm 2 \times 10^{-23}$
V	$9 \times 10^{-25} \pm 1 \times 10^{-25}$

than olivine applied in a core study by Renforth et al. (2015). However the release of Mg in this study ($10^{-19.31\pm0.02}$ mol(Mg) cm^{-2} s^{-1}) was 3 orders of magnitude slower than Mg dissolution calculated by Renforth et al. (2015) ($10^{-15.5}$ to $10^{-16.4}$ mol(Mg) cm^{-2} s^{-1}) and ~2 orders of magnitude slower than Mg dissolution calculated in an olivine-treated pot study by Amann et al. (2020) ($10^{-16.8}$ to $10^{-17.4}$ mol(Mg) cm^{-2} s^{-1}). This indicates SiO_2 polymerisation in basalt minerals retards dissolution relative to fast-weathering olivine.

In summary, slower release of ions into the dissolved form is observed in this core study than in previous observation studies. This may be explained by several processes, including SiO_2 polymerisation, sorption, the formation of secondary minerals which reabsorb ions, and by the lower water fluxes of this study, conducted under natural precipitation and evaporation.

4.2. Alkalinity flux

The flux of ions into solution during dissolution allows calculation of the flux of conservative alkalinity which, as this must be matched by carbonate alkalinity, is the driver of CO_2 removal and the key measure for the rate of enhanced weathering. Alkalinity flux represents the net effect of basalt dissolution and is unaffected by the inherently complex mineralogy of basalt which may undergo preferential phase dissolution (Kelland et al., 2020). Alkalinity flux is calculated directly from dissolved ion-balance, and ions removed from solution by adsorption and precipitation do not contribute to alkalinity flux (Drever, 1997). Here we simplify conservative alkalinity by considering only the four most concentrated cations in basalt (Ca, K, Mg, Na). This is reasonable because other cations are present (and released) at much lower concentrations, and because there is very limited release of free anions from weathering of basalt. Basalt used in this study contained trace carbonate minerals (<1 wt%) so it is assumed dissolved cations derived from silicate weathering.

The flux of alkalinity into solution, $Alk_{surface\ area}$, (eq cm^{-2} s^{-1}) was calculated using eq. (4);

$$Alk_{surface\ area} = \frac{Q\ .\ (\sum([Ca]+[Mg]+[K]+[Na])_{treated-control})}{M\ .\ SA_{basalt}} \quad (4)$$

The concentration of dissolved cations ([Ca], [K], [Mg], [Na]) in the soil pore-waters was averaged across the whole length of triplicate cores for the five sampling events (eq g^{-1}). The sum of dissolved alkalinity in

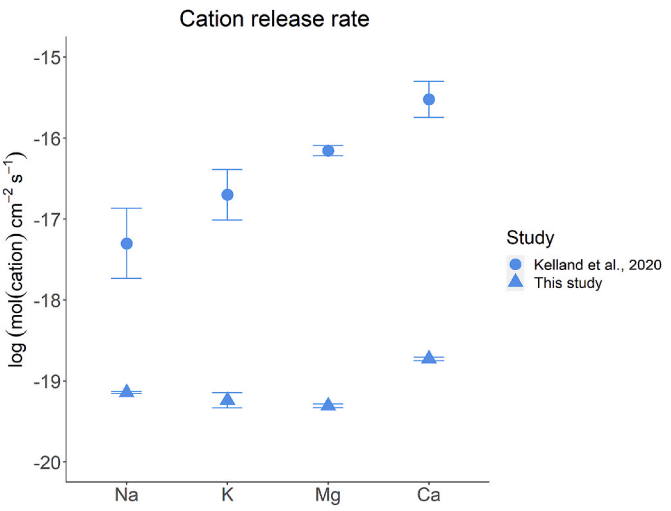

Fig. 4. BET surface-area-normalised ion release rate (mol cm^{-2} s^{-1}) of major elements in basalt, calculated from dissolved cations in this study (triangles) and cations in the soil-plant-water system in Kelland et al. (2020) (circles).

control cores was subtracted from the sum of dissolved alkalinity in treated cores, and multiplied by the infiltration rate (Q, 1.4 × 10^{-5} g s^{-1}). The alkalinity flux was normalised to the BET surface-area of basalt, whereby M is the mass of basalt added to each core (79 g) and SA_{basalt} is the BET site-specific-surface-area of basalt (16.3 × 10^{4} cm^{2} g^{-1}). The surface-area-normalised alkalinity flux was 10$^{-18.22\pm0.03}$ eq cm^{-2} s^{-1}, 62% of which derived from Ca release. This is two to three orders of magnitude slower than the BET-normalised alkalinity flux of dissolved Mg (10$^{-16.1}$ to 10$^{-15.2}$ eq cm^{-2} s^{-1}) in a similar olivine-treated core study by Renforth et al. (2015).

The alkalinity flux was also normalised to the area of land over which basalt was applied, $Alk_{land\ area}$, (eq ha^{-1} yr^{-1}) using eq. (5). This normalisation circumvents the inherent uncertainty in measuring mineral surface areas, and is more directly useful for assessment of the impact of enhanced weathering on carbon fluxes.

$$Alk_{land\ area} = \frac{Q\ .\ T\ .\ (\sum([Ca]+[Mg]+[K]+[Na])_{treated-control})}{SA_{land}} \quad (5)$$

where T is the time in one year (s) and SA_{land} is the surface area of the soil core (7.9 × 10^{-7} ha). The land-area-normalised alkalinity flux measured in this study was 310 ± 30 eq ha^{-1} yr^{-1}, for the application rate of 100 t ha^{-1} used in this study.

4.3. Basalt dissolution

Ion and alkalinity fluxes into solution are the driver of CO_2 consumption, but it is also of interest to assess the rate at which applied basalt dissolves and accumulates in the soil. The rate of ion release is influenced by the relative abundance of each element in basalt. To constrain the surface-area-normalised dissolution rate of basalt, Wr_{basalt}, (g(basalt) cm^{-2} s^{-1}) the ion release rate of each element was normalised to the molar concentration of the respective element in basalt (Eq. (6));

$$Wr_{basalt} = \frac{Wr_{surface\ area\ (x)}}{M_{(x)}} \quad (6)$$

where $Wr_{surface\ area(x)}$ is the surface-area-normalised ion release rate (mol (ion) cm^{-2} s^{-1}) and $M_{(x)}$ is the molar concentration of the respective element in basalt (mol g^{-1}). In doing so, remaining variation in the dissolution rate of basalt relates to mineral differences.

Assuming differences in soil solution are solely a consequence of basalt weathering, the dissolution rate of basalt in soil in this study calculated from dissolved Ca is 10$^{-15.93\pm0.05}$ g(basalt) cm^{-2} s^{-1} and is broadly consistent when considering the release of other major cations (10$^{-15.9\pm0.2}$ g(basalt) cm^{-2} s^{-1}, Mg, K; 10$^{-15.8\pm0.2}$ g(basalt) cm^{-2} s^{-1}, Na). This suggests mineral phases in basalt applied in this study dissolve at a similar rate and differs from model results by Kelland et al. (2020) which suggest olivine and diopside undergo preferential dissolution. Basalt dissolution in this study is approximately 10–100 times slower than olivine dissolution recorded in a similar core study by Renforth et al. (2015) (10$^{-13.7}$ to 10$^{-14.6}$ g(olivine) cm^{-2} s^{-1}).

To assess the timescale on which basalt will undergo complete dissolution, a shrinking core model (SCM) was applied to spherical basalt grains using the equation described by Hangx and Spiers (2009) (Eq. (7));

$$X(t) = \frac{D_0^3 - (D_0 - 2\ .\ Wr\ .\ V_m\ .\ t)^3}{D_0^3} \quad (7)$$

where $X(t)$ is the amount of basalt to have dissolved (vol%), D_0 is the initial particle diameter (cm), t is the dissolution time (s), and V_m is the molar volume (91.6 cm^3 mol^{-1}). Wr is the molar dissolution rate of basalt grains (10$^{-18.3}$ mol(basalt) cm^{-2} s^{-1}) calculated from the dissolution rate of basalt described above (10$^{-15.93\pm0.05}$ g(basalt) cm^{-2} s^{-1}) and the molecular mass of basalt weighted to the mineral composition described in Kelland et al. (2020) (226.6 g mol^{-1}).

The SCM indicates uniform dissolution of 125–250 μm grains will undergo complete (100%) dissolution in 10^6 years, and slow basalt dissolution will require extensive comminution (0.02 μm particles) for basalt to completely dissolve within 1000 years. In light of this, the accumulation of basalt in agricultural soil must be considered when planning basalt addition in multiple years.

4.4. Implications for agricultural soil

The co-benefits of basalt addition on long-term soil quality has been discussed by other authors (Swoboda et al., 2021). Here we highlight the short-term impact from the accumulation of undissolved residual basalt in the ploughed layer following repeated annual addition. Applying the dissolution rate observed in this study to the SCM discussed in section 4.3 indicates that, even if basalt were ground to 1 μm diameter, <1% basalt would dissolve in one year. Consequently, most of the added basalt will remain in the soil and, if further basalt is added annually, progressively accumulate in the top soil of arable land to alter physical, chemical and biological soil properties. The addition of basalt at 100 t ha^{-1} is the equivalent of a 4.8 mm yr^{-1} layer (assuming a 40% porosity, as seen in the soil). With a typical ploughed layer 20 cm thick, it would take only 20 years of sequential addition before half of the soil consisted of undissolved basalt. Considering the proposed addition of enhanced weathering to actively cultivated arable land, it is essential to prevent large-scale basalt application impairing soil structure, cation exchange capacity (CEC), soil microorganisms and overall soil quality. In light of this, annual basalt application may need to be limited to ≈5 years to prevent the accumulation of residual basalt exceeding 10% of the ploughed layer. In practice, it is unlikely that basalt would be continuously added to agricultural soil if the carbon removal benefit was negligible.

It is also important to consider the long-term impact of secondary phase precipitation or changes in exchangeable ion chemistry in the soil as a result of basalt addition. Depleted Al, Ba, Fe, Mn, and Si in soil solution suggest dissolved ions were removed from solution via sorption or secondary formation of minerals such as clays and Al-, Fe-oxides (as seen in previous studies; Panhwar et al., 2016). The precipitation of clays and iron oxides from dissolved ions could impact physical and chemical properties of the soil core. For example, precipitation of clays and hydrous Fe oxides has been shown to reduce heavy metal availability by exchange or adsorption which, in turn, reduces the risk of plant toxicity (Bradl, 2004; Berner and Berner, 2012; Igbokwe and Ugwu, 2018). In addition, the large, charged surface-area of clays

increases the CEC of soil which has been shown to improve nutrient retention, and the retention of K+ as an interlayer cation within secondary clays could provide a long term K supply, an essential macronutrient for plant growth (Basak et al., 2016). Precipitation of clays and metal oxides could also influence physical properties of the soil core, reduce soil erosion, and improve water and soil organic carbon retention (Edwards et al., 2017). Nevertheless, the precipitation of oxides on negatively charged sites has the potential to reduce soil CEC (Sumner, 1963; Durn et al., 2019).

Depending on the composition of the applied treatment, large-scale enhanced weathering deployment could elevate the heavy metal content of soil pore-water and pose an environmental risk (Beerling et al., 2018). In this study, the concentration of dissolved heavy metals averaged across the treated core (2.4 ± 0.1 ppb, Ni; 0.32 ± 0.02 ppb, Cr; 4.7 ± 0.4 ppb, V) were not enriched beyond the safety threshold of drinking water (Gautam et al., 2014), or freshwater (Environment Agency, 2009). Moreover, the release of low levels of V and Cr has been shown to have beneficial effects on plant growth (Chen et al., 2021) and soil microorganisms (Singh and Kalamdhad, 2011). Although basalt dissolution measured in this study does not pose an immediate contamination risk to surrounding ground- and fresh-water environments, large-scale EW deployment will require comprehensive monitoring practices to ensure residual basalt and secondary mineral formation do not impair the quality of arable soils.

4.5. CO_2 drawdown

The flux of alkalinity released to the dissolved phase by basalt dissolution provides a direct quantitative measurement of the carbon dioxide removal (CDR) potential of basalt. This was calculated, using eq. (8), in terms of $kgCO_2\ ha^{-1}\ yr^{-1}$;

$$CDR = Alk_{land\ area} \cdot M_{Co2} \cdot \eta \cdot \frac{1}{1000} \quad (8)$$

where $Alk_{land\ area}$ is the alkalinity flux normalised to land-area (310 eq $ha^{-1}yr^{-1}$ see Section 4.2); M_{Co2} is the molecular mass of CO_2 (44 g mol^{-1}); η is the molar ratio of CO_2 removed from the atmosphere relative to alkalinity released during enhanced weathering. Here we used η = 0.75, as in Renforth (2019), to account for the conversion of some HCO_3^- to CO_3^{2-} in the river and ocean system. Pedogenic carbonate formation was not assessed within the scope of this study, therefore carbon drawdown relates to sequestration into dissolved forms. These calculations do not consider emissions released over the life-cycle of EW from mining, transport and comminution which have been previously estimated to reduce the net drawdown potential of EW by 10–30% (Moosdorf et al., 2014; Lefebvre et al., 2019).

After a single application, the CDR potential of basalt was 10.2 ± 0.8 $kgCO_2\ ha^{-1}\ yr^{-1}$. This rate of drawdown is ~200 fold slower than CO_2 uptake calculated in biotic, basalt-treated mesocosm studies, conducted at two rates of basalt addition: 100 t ha^{-1} (2000 $kgCO_2\ ha^{-1}\ yr^{-1}$; Kelland et al., 2020) and 50 t ha^{-1} (1830 $kgCO_2\ ha^{-1}\ yr^{-1}$; Vienne et al., 2022). Lower CDR observed in this study reflects the complexity of the soil-mineral-fluid system in the soil conditions used, and a substantially lower water flux under our natural conditions than used in previous studies. Water fluxes applied in previous mesocosm and modelling studies (Renforth et al., 2015; Amann et al., 2020; Kelland et al., 2020; Kantzas et al., 2022; Vienne et al., 2022) include irrigation and are over an order of magnitude greater than the flux of water measured through soil cores in this study.

Water is a primary requirement for weathering and dissolution, and the flux of water is known to limit both the dissolution of minerals and the transport of dissolution products. The extent to which water flux controls the slower dissolution and CDR potential in this study than in previous irrigated studies can be assessed by comparing rates of CDR normalised to the flux of water (i.e. kg of CO_2 uptake, per land-area, per mm of water flux). Values for this study, with a natural water flux through the cores of 57 mm yr^{-1}, are 0.2 $kgCO_2\ ha^{-1}\ mm^{-1}$, while those in the Kelland et al. (2020) study, with an irrigated flux of 767 mm yr^{-1}, is 2.6 $kgCO_2\ ha^{-1}\ mm^{-1}$. Even when normalising for water flux in this way, CO_2 uptake rates in this study are ≈15 times lower than in the earlier mesocosm studies. This indicates that other factors limit dissolution, perhaps indirectly related to water flux. These may include natural drying/wetting cycles creating a saturation limitation on dissolution at the mineral-water interface, increased secondary uptake of ions in the soil, or preferential flow of the limited water through channels in the natural soil environment. It is possible the regular irrigation regime applied in existing pot/core studies (Renforth et al., 2015; Amann et al., 2020; Kelland et al., 2020; Vienne et al., 2022) optimised mineral-fluid interaction, whereas real-time variation in rainfall patterns may have inhibited dissolution in this core study.

In summary, CDR rates assessed in the natural conditions of Oxfordshire are much lower than those assessed in previous lab and modelling studies, with the lower water flux observed in our natural settings a major control on these lower CDR rates.

5. UK impact

The CDR potential of large-scale enhanced weathering deployment can be calculated by assuming the alkalinity flux derived in this study is representative of that in basalt-treated agricultural fields more generally. We limit continuous annual application to five years to prevent accumulation of undissolved basalt in cultivated soils exceeding 10% of the ploughed layer (Section 4.4). If all UK soils behave identically to those in this study, applying 100 t ha^{-1} per year of ground basalt for five years to all UK croplands (6.1 Mha; DEFRA, 2020) would remove 0.31 ± 0.02 $MtCO_2\ yr^{-1}$ from the atmosphere, with this level of removal continuing effectively indefinitely. Further application onto all farmland (17.1 Mha; DEFRA, 2020), including non-ploughed grazed land, may increase drawdown to 0.87 ± 0.07 $MtCO_2\ yr^{-1}$, though the rate of weathering without mixing into the soil is not well constrained by this study.

Hydrological conditions vary significantly across the UK (Kay et al., 2013) and, given our conclusion that water-flux is a critical control on the rate of enhanced weathering, this variation should be considered in extrapolating nationally from our experiment. To do so, we use river flow data ($m^3\ s^{-1}$) from the National River Flow Archive (NRFA, 2022) to understand the net water flux available for EW following rainfall, evapotranspiration and irrigation. Using river fluxes for this purpose ignores groundwater recharge, but this is minor (<10%) relative to river fluxes (Jackson et al., 2013). Averaging UK river fluxes, normalised by crop-cover in catchment areas, indicates a weighted net water flux of 235 mm yr^{-1} (NRFA, 2022). This is approximately four times greater than the water flux measured in Oxfordshire during this study (57 mm yr^{-1}). Assuming a linear relationship between water flux and CDR potential, and increasing the flux above for all arable land accordingly, suggests 1.3 ± 0.1 $MtCO_2\ yr^{-1}$ as a best estimate for the drawdown potential of EW in the UK when accounting for variation in hydrology. This is equivalent to 3% of current greenhouse gas emissions from UK agriculture (which were 46.3 $MtCO_2e\ yr^{-1}$ in 2019; DEFRA, 2021a). It is likely that the relationship between water flux and CDR potential is not linear due to the complex interplay between dissolution, alkalinity release and natural drying/wetting cycles, particularly in dry conditions. Further research into this issue is required before a more accurate assessment of total UK EW potential can be made.

The rate of CDR calculated from this empirical study is 5- to 25- fold slower than derived in the detailed modelling study of Kantzas et al. (2022) (6–30 $MtCO_2\ yr^{-1}$). That study considered lower application rates of basalt (40 t ha^{-1} yr-1), but with addition at this rate for multiple years with the annual CDR rate derived at a steady state condition. A large component of the higher CDR potential in Kantzas et al. (2022) is likely to be due to high water fluxes applied in that model for the UK

(461–849 mm yr^{-1}); rates significantly higher than net water fluxes derived from river flow in arable areas.

Addition of silicates such as basalt to agricultural land has been practised in various parts of the world for many years, and can have important agricultural advantages for nutrient supply and retention (Swoboda et al.,2021). There may be benefit from expanding such application for agricultural reasons, but the capacity of this action for draw down of CO_2 from the atmosphere should not be overstated as a reason for such addition.

6. Conclusion

As negative emission technologies are increasingly relied upon to reduce atmospheric greenhouse gases, it is important to understand the contribution enhanced weathering could make to UK net-zero emission reduction targets. This soil core study revealed the fate of dissolution products at a range of depths within UK agricultural soil cores treated with crushed basalt and exposed to natural UK weather. Basalt dissolution elevated the dissolved concentration of major cations (Ca, Na, Mg, and K), and increased the alkalinity flux into the soil-water system at a rate of 310 ± 30 eq ha^{-1} yr^{-1} when considering the high application rate used in this study (100 t ha^{-1}). Assuming findings in this core study are representative of the field scale, basalt dissolution in natural agricultural soil has the potential to draw down 10.2 ± 0.8 $kgCO_2$ ha^{-1} yr^{-1} after a single application. Slow, water-limited dissolution and accumulation of undissolved basalt in the ploughed layer could limit multiple additions. We calculate that five years of annual basalt application at 100 t ha^{-1} has the potential to sequester 1.3 ± 0.1 $MtCO_2$ yr^{-1} over UK cropland. This value takes into account hydrological variations, which this study indicates are a critical control on CO_2 removal potential. The resulting flux is equivalent to <3% of UK agricultural emissions and is substantially lower than previous modelled estimates (Kantzas et al., 2022). Given the importance of water flux demonstrated in this study, future work is needed to understand the interaction between these fluxes and enhanced weathering across a range of soil types.

Declaration of competing interest

The authors declare that they have no known competing financial interests or personal relationships that could have appeared to influence the work reported in this paper.

Data availability

Data will be made available on request.

Acknowledgments

The authors would like to thank Clare Hill (FAI Farms), Rob Ainsworth, Graeme Jackson (Soils Limited) for their help with soil core extraction; James King and Cornelius Vermaak for help with experimental set-up; Colin Johnston, Steve Wyatt, Jane Barling (University of Oxford) for help during analysis. The work was supported by the NERC environmental research doctoral training partnership at the University of Oxford (Grant NE/L002612/1).

Appendix A. Supplementary data

Supplementary data to this article can be found online at https://doi.org/10.1016/j.apgeochem.2022.105482.

References

Amann, T., et al., 2020. Enhanced Weathering and related element fluxes - a cropland mesocosm approach. Biogeosciences 17 (1), 103–119. https://doi.org/10.5194/bg-17-103-2020.

Basak, B.B., et al., 2016. Bio-intervention of naturally occurring silicate minerals for alternative source of potassium: challenges and opportunities. Adv. Agron. https://doi.org/10.1016/bs.agron.2016.10.016.

Beerling, D.J., et al., 2018. Farming with crops and rocks to address global climate, food and soil security. Nat. Plants 4, 138–147. https://doi.org/10.1038/s41477-018-0108-y.

Beerling, D.J., et al., 2020. Potential for large-scale CO 2 removal via enhanced rock weathering with croplands. Springer US Nature 583. https://doi.org/10.1038/s41586-020-2448-9. May 2018.

ten Berge, H.F.M., et al., 2012. Olivine weathering in soil, and its effects on growth and nutrient uptake in ryegrass (Lolium perenne L.): a pot experiment. PLoS One 7 (8). https://doi.org/10.1371/journal.pone.0042098.

Berner, R.A., Berner, E.K., 2012. Chemical weathering: minerals, plants and water chemistry. In: Global Environment: Water, Air, and Geochemical Cycles, second ed. second ed. Princeton University Press.

Berner, R.A., 1999. A new look at the long-term carbon cycle. GSA Today (Geol. Soc. Am.) 9 (11), 1–6.

Bradl, H.B., 2004. Adsorption of heavy metal ions on soils and soils constituents. J. Colloid Interface Sci. 277 (1), 1–18. https://doi.org/10.1016/j.jcis.2004.04.005.

Brantley, S.L., Mellot, N.P., 2000. Surface area and porosity of silicates. Am. Mineral. 85 (1990), 1767–1783.

Chen, L., et al., 2021. Vanadium in soil-plant system: source, fate, toxicity, and bioremediation. June J. Hazard Mater. 405, 124200. https://doi.org/10.1016/j.jhazmat.2020.124200. Elsevier B.V.

DEFRA, 2020. Farming Statistics – Provisional Arable Crop Areas, Yields and Livestock Populations at 1 June 2020 United Kingdom. Department for Environment. *Food and Rural Affairs*, (June), p. 29. Available at: https://assets.publishing.service.gov.uk/government/uploads/system/uploads/attachment_data/file/651173/structure-jun2017prov-UK-12oct17.pdf.

DEFRA, 2021. Agri-climate report. Westminster. Available at: https://www.gov.uk/government/statistics/agri-climate-report-2021/agri-climate-report-2021#key-messages.

Drever, J.I., 1997. The Geochemistry of Natural Waters: Surface and Groundwater Environments. Prentice Hall, Upper Saddle River, N.J.

Durn, G., et al., 2019. Impact of iron oxides and soil organic matter on the surface physicochemical properties and aggregation of Terra Rossa and Calcocambisol subsoil horizons from Istria (Croatia). Catena 183. https://doi.org/10.1016/j.catena.2019.104184. August 2018.

Edwards, D.P., et al., 2017. Climate change mitigation: potential benefits and pitfalls of enhanced rock weathering in tropical agriculture. Biol. Lett. 13 (4) https://doi.org/10.1098/rsbl.2016.0715.

Environment Agency, 2009. Selected Water Quality Standards. Hydro-geological Risk Assessment for Landfills, pp. 75–80, 1989.

Fuss, S., et al., 2018. Negative emissions - Part 2: costs, potentials and side effects. Environ. Res. Lett. 13 (6) https://doi.org/10.1088/1748-9326/aabf9f.

Gautam, R.K., et al., 2014. Heavy Metals in Water: Presence, Removal and Safety. Royal Society of Chemistry, pp. 1–24. https://doi.org/10.1039/9781782620174-00001.

Hangx, S.J.T., Spiers, C.J., 2009. Coastal spreading of olivine to control atmospheric CO2 concentrations: a critical analysis of viability. Int. J. Greenh. Gas Control 3 (6), 757–767. https://doi.org/10.1016/j.ijggc.2009.07.001.

Hartmann, J., et al., 2013. Enhanced chemical weathering as a geoengineering strategy to reduce atmospheric carbon dioxide, supply nutrients, and mitigate ocean acidification. Rev. Geophys. 51, 113–149. https://doi.org/10.1002/rog.20004.1. Institute, 2012.

Igbokwe, O.A., Ugwu, I.M., 2018. Sorption of Heavy Metals on Clay Minerals and Oxides: A Review, vol. 2. Intech open, p. 64. https://doi.org/10.5772/32009.

Jackson, C.R., Macaky, J.D., Bloomfield, J.P., 2013. In: A climate change report card for water Working Technical Paper 1 . Changes in groundwater levels , temperature and quality in the UK over the 20 th century : an assessment of evidence of impacts from climate change, pp. 1–14. Available at: http://nora.nerc.ac.uk/503271/.

Kantzas, E.P., et al., 2022. Substantial carbon drawdown potential from enhanced rock weathering in the United Kingdom. Nat. Geosci. https://doi.org/10.1038/s41561-022-00925-2. Springer US.

Kay, A., et al., 2013. A hydrological perspective on evaporation: historical trends and future projections in Britain. J. Water Clim. Change 4 (3), 193–208. https://doi.org/10.2166/wcc.2013.014.

Kelemen, P.B., et al., 2020. Engineered carbon mineralization in ultramafic rocks for CO2 removal from air: Review and new insights. Chem. Geol. 550.

Kelland, M.E., et al., 2020. Increased yield and CO2 sequestration potential with the C4 cereal Sorghum bicolor cultivated in basaltic rock dust-amended agricultural soil. Global Change Biol. 26 (6), 3658–3676. https://doi.org/10.1111/gcb.15089.

Lefebvre, D., et al., 2019. Assessing the potential of soil carbonation and enhanced weathering through Life Cycle Assessment: a case study for Sao Paulo State, Brazil. J. Clean. Prod. 233, 468–481. https://doi.org/10.1016/j.jclepro.2019.06.099. Elsevier Ltd.

Manning, D.A.C., 2008. Biological enhancement of soil carbonate precipitation: passive removal of atmospheric CO2. Mineral. Mag. 72 (2), 639–649. https://doi.org/10.1180/minmag.2008.072.2.639.

Moosdorf, N., Renforth, P., Hartmann, J., 2014. Carbon dioxide efficiency of terrestrial enhanced weathering. Environ. Sci. Technol. 48 (9), 4809–4816. https://doi.org/10.1021/es4052022.

NRFA, 2022. UK National River flow archive. Available at: https://nrfa.ceh.ac.uk/web-download-service. (Accessed 4 September 2022).

Palandri, J.L., Kharaka, Y.K., 2004. A Compilation of Rate Parameters of Water-Mineral Interaction Kinetics for Application to Geochemical Modeling, vols. 2004–1068. USGS Open File Report, p. 71. https://doi.org/10.1098/rspb.2004.2754.

Panhwar, Q.A., et al., 2016. Applying limestone or basalt in combination with bio-fertilizer to sustain rice production on an acid sulfate soil in Malaysia. Sustainability 8 (7). https://doi.org/10.3390/su8070700.

Renforth, P., 2019. The negative emission potential of alkaline materials. Nat. Commun. 10 (1), 1–29. https://doi.org/10.1038/s41467-019-09475-5.

Renforth, P., Pogge von Strandmann, P.A.E., Henderson, G.M., 2015. The dissolution of olivine added to soil: implications for enhanced weathering. Appl. Geochem. 61, 109–118. https://doi.org/10.1016/j.apgeochem.2015.05.016. Elsevier Ltd.

SEIFRITZ, W., 1990. CO2 disposal by means of silicates. Nature. https://doi.org/10.1038/345486b0, 486–486.

Singh, J., Kalamdhad, A.S., 2011. Effects of heavy metals on soil, plants, human health and aquatic life. Int. J. Res. Chem. Environ. 1 (2), 15–21. Available at: https://www.researchgate.net/publication/265849316_Effects_of_Heavy_Metals_on_Soil_Plants_Human_Health_and_Aquatic_Life.

Smith, P., et al., 2015. Biophysical and economic limits to negative CO2 emissions', *Nature Climate Change*. Nat. Publ. Group 6 (1), 42–50. https://doi.org/10.1038/nclimate2870.

Strefler, J., et al., 2018. Potential and costs of carbon dioxide removal by enhanced weathering of rocks. Environ. Res. Lett. 13 (3), 034010 https://doi.org/10.1088/1748-9326/aaa9c4.

Sumner, M.E., 1963. Effect of iron oxides on positive and negative charges in clays and soils. Clay Miner. 5 (29), 218–226. https://doi.org/10.1180/claymin.1963.005.29.08.

Swoboda, P., Döring, T.F., Hamer, M., 2021. 'Remineralizing Soils? the Agricultural Usage of Silicate Rock Powders: A Review', *Science Of the Total Environment*. Elsevier B.V., 150976 https://doi.org/10.1016/j.scitotenv.2021.150976 xxxx.

Tester, J.W., et al., 1993. Correlating quartz dissolution kinetics in pure water from 25" to 625°C. In: Proceedings, Eighteenth Workshop on Geothermal Reservoir Engineering, pp. 213–224.

The Royal Society and Royal Academy of Engineering, 2018. Greenhouse Gas Removal.

UKCEH, 2021. Potential evaporation and precipitation, Chimney meadows. Available at: https://cosmos.ceh.ac.uk/sites/CHIMN.

Vienne, A., Poblador, S., Portillo-Estrada, M., Hartman, H., 2022. Enhanced weathering using basalt rock powder: carbon sequestration, Co-benefits and risks in a mesocosm study with Solanum tuberosum. Front. Clim. https://doi.org/10.3389/fclim.2022.869456.

Walker, J.C.G., Hays, P.B., Kasting, J.F., 1981. A negative feedback mechanism for the long-term stabilization of EARTH'S surface temperature. J. Geophys. Res. 86 (20), 9776–9782. https://doi.org/10.1029/JC086iC10p09776.

White, A.F., Brantley, S.L., 2003. The effect of time on the weathering of silicate minerals: why do weathering rates differ in the laboratory and field? Chem. Geol. 202 (3–4), 479–506. https://doi.org/10.1016/j.chemgeo.2003.03.001.